AIP | Journal of Applied Physics

Electrical properties of thermoelectric cobalt Ca3Co4O9 epitaxial heterostructures

Haizhong Guo, Shufang Wang, Le Wang, Kui-juan Jin, Shanshan Chen et al.

Citation: J. Appl. Phys. **113**, 113707 (2013); doi: 10.1063/1.4795767
View online: http://dx.doi.org/10.1063/1.4795767
View Table of Contents: http://jap.aip.org/resource/1/JAPIAU/v113/i11
Published by the American Institute of Physics.

Electrical properties of thermoelectric cobalt $Ca_3Co_4O_9$ epitaxial heterostructures

Haizhong Guo,[1] Shufang Wang,[2,a)] Le Wang,[1] Kui-juan Jin,[1,b)] Shanshan Chen,[2] Guangsheng Fu,[2] Chen Ge,[1] Huibin Lu,[1] Can Wang,[1] Meng He,[1] and Guozhen Yang[1]
[1]*Beijing National Laboratory for Condensed Matter Physics, Institute of Physics, Chinese Academy of Sciences, Beijing 100190, People's Republic of China*
[2]*College of Physics Science and Technology, Hebei University, Baoding 071002, People's Republic of China*

(Received 25 December 2012; accepted 4 March 2013; published online 18 March 2013)

Heterostructures fabricated from layered cobalt oxides offer substantial advantages for thermoelectric applications. *C*-axis-oriented $Ca_3Co_4O_9$ (CCO) thin films on $SrTiO_3$ substrates and $Ca_3Co_4O_9/SrTi_{0.993}Nb_{0.007}O_3$ *p-n* heterojunctions were fabricated by pulsed laser deposition. The measurements of in-plane resistivity, thermopower, and magnetic properties performed on the $Ca_3Co_4O_9$ thin films were found to be comparable to *ab*-plane those of the single crystals due to good orientation of the films. The temperature dependence of the electrical transport properties of $Ca_3Co_4O_9/SrTi_{0.993}Nb_{0.007}O_3$ *p-n* heterojunction was also investigated. The junction shows two distinctive transport mechanisms at different temperature regimes under forward bias: tunneling across the Schottky barrier in the temperature range of 100-380 K, and tunneling mechanism at low bias and thermal emission mechanism at high bias between 10 and 100 K. However, for the case of low reverse bias, the trap assisted tunneling process should be considered for the leakage current. Negative magnetoresistance effect is observed at low temperatures, related to the electron spin-dependent scattering and the interface resistance of the heterostructures. © *2013 American Institute of Physics*. [http://dx.doi.org/10.1063/1.4795767]

I. INTRODUCTION

In recent years, fabrication of nanoscale magnetic heterostructures, including manganese oxide heterostructures[1–4] and magnetic metal thin films,[5,6] has attracted a great deal of interests due to its variety of magnetic applications since discovery of giant magnetoresistance (GMR) in metallic multilayers[7] and colossal magnetoresistance (CMR) in doped manganites.[1,8] Owing to the dependence of properties on direction, it is often optimal to grow functional oxides in particular directions to maximize their properties for a specific application. With recent advances in deposition techniques, including pulsed-laser deposition (PLD) and reactive molecular-beam epitaxy (MBE), high-quality magnetic heterostructures have been fabricated, which have enabled the fabrication of artificial multifunctional materials.[9–12] At the same time, they have exposed a wealth of phenomena at the boundaries where compounds with different structural instabilities and electronic properties meet, giving unprecedented access to new physics emerging at interfaces.[4,13,14]

Layered cobalt oxide $Ca_3Co_4O_9$ (CCO) has attracted great attentions as one of candidates for thermoelectric applications due to its excellent thermoelectric performance.[15] Its crystal structure consists of alternating layers of the triple rocksalt-type Ca_2CoO_3 subsystem and the single CdI_2-type CoO_2 subsystem stacked along the *c*-axis.[15] Thin-film thermoelectric materials offer tremendous scope for thermoelectric performance enhancement involving the use of quantum-confinement effects and phonon-blocking/electron-transmitting superlattices, or basing on thermionic effects in heterostructure.[16] In particular, thin films and heterostructures would provide the possibility of externally modifying the properties by epitaxial strain or artificial boundaries, and thus potentially generating novel properties at the interfaces, opens a new perspective for a variety of very important experimental investigations.[9] In this work, we have grown the *c*-axis-oriented $Ca_3Co_4O_9$ thin films and $Ca_3Co_4O_9/SrTi_{0.993}Nb_{0.007}O_3$ *p-n* heterojunctions by PLD. The in-plane resistivity, thermopower, and magnetic properties of the CCO thin films were investigated, and the electrical transport properties of the CCO/Nb-doped $SrTiO_3$ (SNTO) junctions were also measured.

II. EXPERIMENTS

Epitaxial CCO films (200 nm thick) were grown on $SrTiO_3$ (STO) and 0.7 wt. % SNTO (001) substrates by PLD.[17] The films were deposited at 680 °C using an excimer XeCl laser (308 nm, 3 Hz) at oxygen pressure of 40 mTorr and then postannealed at 820 °C for 60 min under the flowing oxygen. The crystalline quality of the CCO/SNTO heterostructure was analyzed using x-ray diffraction (XRD) spectrometer with Cu $K\alpha$ radiation. Resistivity measurements were performed using a Physical Properties Measurement System (PPMS, Quantum Design Inc.). The standard four-point probe method (shown in the inset of Fig. 2(a)) was used to measure in-plane resistivity (ρ_{ab}) of the CCO film grown on STO substrate. To make the ohmic contact, four platinum electrodes (0.5 mm diameter) were deposited onto the films via thermal evaporation. The measurements of the temperature dependences of the Hall effect, magnetic susceptibility, current-voltage characteristics, and thermopower were also performed using PPMS system in the range of 5-380 K.

a)E-mail: swang2008@hotmail.com.
b)E-mail: kjjin@aphy.iphy.ac.cn.

III. RESULTS AND DISCUSSIONS

The XRD θ-2θ scan curve of CCO/SNTO heterostructure is shown in Fig. 1. Besides the peak from SNTO (00 l) substrate, only peaks from diffractions of (00 l) CCO planes are observed, and no diffraction peaks from secondary phases or randomly oriented grains are observed, indicating that the thin films are grown along the c-axis with a good single phase. The ω scan of the CCO (004) peak, shown in inset of Fig. 1, shows a full width at half maximum (FWHM) of 0.31°, indicating the excellent c-axis orientation. Moreover, from XRD results, it is calculated that the c-axis lattice constant is 10.065 Å, close to the bulk value of 10.833 Å.[9] Similar value have been previously reported for $Ca_3Co_4O_9$ thin films.[18,19] $Ca_3Co_4O_9$ is a misfit-layered oxide consisting in two monoclinic subsystems: the hexagonal CoO_2 subsystem and the rocksalt Ca_2CoO_3 subsystem, with identical $a = 4.838$ Å, $c = 10.833$ Å, and $\beta = 98.06°$ parameters, but different b parameter ($b1 = 4.456$ Å for Ca_2CoO_3 subsystem and $b2 = 2.819$ Å for Ca_2CoO_3 subsystem, respectively).[15] Depending on the lattice and symmetry mismatch, the first layer should be the rocksalt Ca_2CoO_3 subsystem on the cubic on $SrTiO_3$ (001) substrate, and it is compatible with the reduced lattice mismatch (~14.2%) between $2a$ of the substrate (7.810 Å) and $\sqrt{2}a$ of the Ca_2CoO_3 subsystem (6.840 Å). The epitaxial growth of the CCO thin films on STO is confirmed by the high-resolution scanning transmission electron microscopy (STEM) images. The inset of Fig. 2(b) shows the STEM imaging near the interface region. It can be seen that the interface is very sharp and coherent, and there is no evidence of secondary phases or any chemical reaction in the interface region over large distances. Sharp interface and no buffer layer existing at the interface of the CCO heterostructures indicates the high quality of our CCO heterostructures grown by PLD.

The temperature dependence of the in-plane resistance (ρ_{ab}) of CCO film on STO substrate was shown in Fig. 2(a). The temperature dependence of the in-plane resistance of the CCO film exhibits a broad minimum around 100 K, exhibiting a broad transport crossover from the high-temperature metallic-like regime to the low-temperature insulating-like

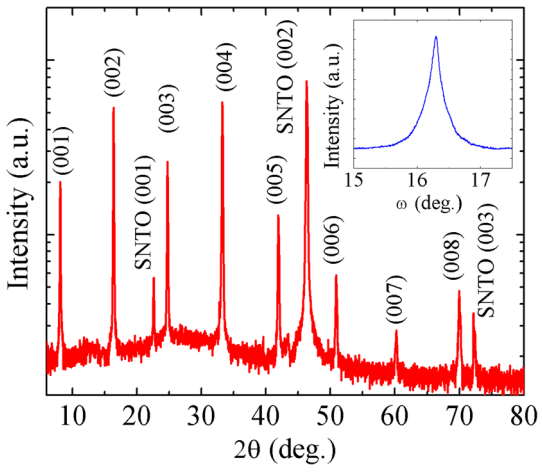

FIG. 1. XRD (a) θ-2θ scan curves and (b) ω scan of the CCO/SNTO heterostructure.

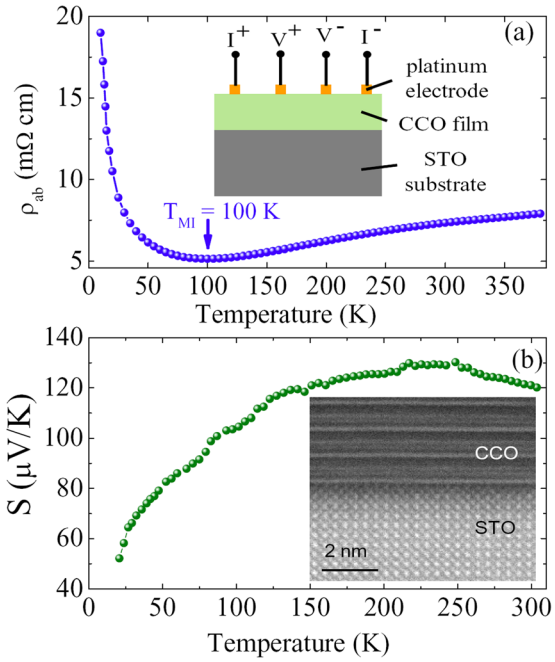

FIG. 2. (a) Temperature dependence of the in-plane resistivity (ρ_{ab}) of the CCO film on the STO substrate, measured with a current of 50 μA. (b) Temperature dependence of S of the CCO films. Inset in Fig. 2(a) shows the schematic illustrations of the CCO film on the STO substrate. Inset in Fig. 2(b) shows a high-resolution STEM imaging near the interface region demonstrating the epitaxial growth of CCO film on STO substrates.

one. The increase in the electrical resistance at low temperature can be attributed to the decrease of the density of states at Fermi level (E_F) with decreasing temperature below 100 K, and opening an energy gap across E_F at a temperature below 50 K.[20] The temperature dependence of the in-plane thermopower (Seebeck S_{ab}) of the CCO thin films is shown in Fig. 2(b). The positive S_{ab} over the measured temperature range indicates that the majority of charge carriers have holelike character, which is consistent with the pervious results on the CCO bulks.[15,21] The values of the ρ_{ab} and S_{ab} at room temperature are about 7 mΩ·cm and 120 μV/K, respectively, comparable to those of $Ca_3Co_4O_9$ single crystal (ρ_{ab} ~ 10-40 mΩ·cm and S_{ab} ~ 125 μV/K),[15] revealing high quality of our samples.

Hall effect measurements as a function of temperature on the CCO thin film on the STO substrate also were performed, as shown in Fig. 3. It can been seen from Fig. 3 that the positive value of the Hall coefficient and positive slope of the Hall resistivity between 5-380 K implying the holelike charge carriers of the CCO thin film, consistent with the results from the thermopower measurements. Hall coefficient R_H exhibits the strong temperature dependence, as shown in Fig. 3(a). The Hall coefficient smoothly decreases with decreasing temperature from 380 K down to around 100 K, and then slowly increases from 100 K to 25 K and exhibits a sudden enhancement below 25 K. This unconventional temperature dependence of the Hall coefficient of the CCO film is believed to be related to the unusual behavior of strongly electron correlations of CCO.[22] The broad crossover of the temperature dependence of the Hall coefficient also occurs at around 100 K. Figures 3(b) and 3(c) show the Hall resistivity ρ_H versus magnetic field below 100 K and above 100 K,

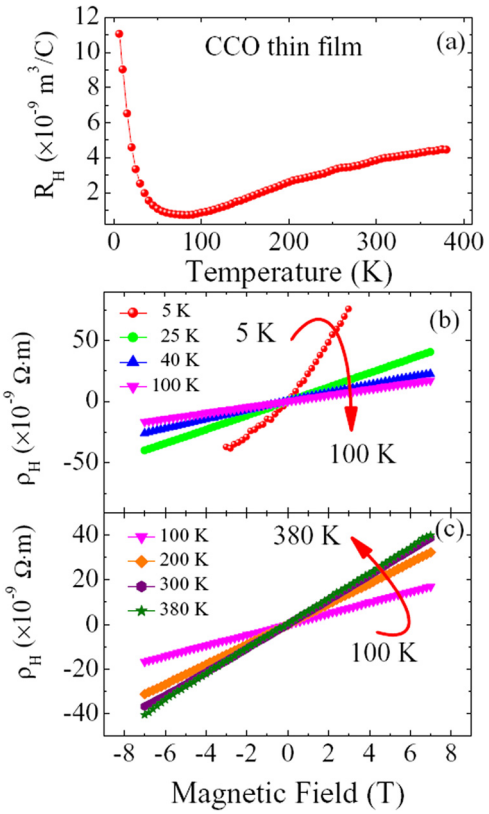

FIG. 3. (a) Temperature dependence of the Hall coefficient R_H of the CCO film on STO substrate under the magnetic field of ±7 T; the Hall resistivity ρ_H versus magnetic field (b) below 100 K and (c) above 100 K.

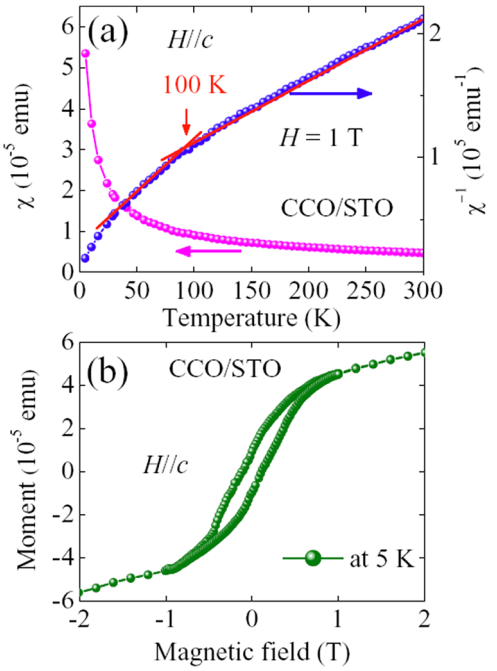

FIG. 4. (a) Temperature dependence of the magnetic susceptibility χ and inverse susceptibility χ^{-1} of the CCO film on STO substrate; χ was measured in the field cooling mode with $H = 1$ T. (b) The relation between the magnetization M and magnetic field H for the CCO film on the STO substrate at 5 K. Red lines correspond to the Curie-Weiss behavior.

respectively. The calculated hole carrier density of the CCO film at room temperature is about $\sim 4.3 \times 10^{20}$ cm^{-3}.

Figure 4 shows the temperature dependence of magnetic susceptibility χ and inverse susceptibility χ^{-1} of the CCO film on the STO substrate measured in the field-cooling mode with $H = 1$ T in the $H//c$ geometries. The magnetization increases monotonically upon cooling down to ~20 K, then increases rapidly with further decreasing temperature, indicating a transition to a ferrimagnetic state occurring at $T \sim 20$ K.[23,24] The ferrimagnetic interaction is parallel to the c axis. Considering the alternating stacking structure of $Ca_3Co_4O_9$ along the c axis, the ferrimagnetism is most likely caused by interlayer coupling between the $[Ca_2CoO_3]$ and $[CoO_2]$ subsystems.[23,24] From the corresponding inverse susceptibility curve (χ^{-1}(T)), the Curie-Weiss law was applied to fit the data, shown as dashed lines in Fig. 4. As temperature decreases from 300 K down to about 100 K, the inverse susceptibility decreases approximately linearly following the Curie-Weiss law well, then there is a clear change of slope below about 100 K. The existence of an incommensurate spin-density-wave (IC-SDW) state below ~100 K was confirmed by positive muon spin rotation and relaxation experiments in the $Ca_3Co_4O_9$ single crystals.[23,24] Therefore, the change in the slope of the temperature dependence of the inverse susceptibility around ~100 K is believed to be related to the transition from a paramagnetic state to IC-SDW state. The broad minimum around 100 K in the temperature dependence of the in-plane resistance of the CCO film suggests that the behavior of conducting electron is strongly affected by the IC-SDW order. The relationship between magnetization M and magnetic field H at 5 K was shown in Fig. 4(b). The magnetic field was applied parallel to the c-axis of the CCO film. The CCO/STO sample displays a clear hysteresis M-H curve, suggesting that the ferrimagnetic interaction is parallel the c axis. In fact, the $Ca_3Co_4O_9$ single crystal exhibits the anisotropic magnetic properties, and a ferrimagnetic hysteresis loop just could be observed for H parallel to the c-axis of the CCO while not for H parallel to the ab-plane of the CCO single crystal.[25]

The junction conductive resistance and the current-voltage (I-V) characteristics measurements on the CCO/SNTO junctions were performed by two-probe technique (shown in the inset of Fig. 6(b)) to avoid the effects of current distribution in the junction. Ohmic contacts were prepared by evaporating circular platinum and silver with the 200-μm-diameter sizes on the CCO and SNTO, respectively. The electrode arrangement is illustrated schematically in the inset of Fig. 6(b), and the polarity of the applied bias is defined as positive when applied to the CCO. Figure 5(a) shows the typical current-voltage (I-V) characteristics of the CCO/SNTO junctions at temperatures varying from 10 to 380 K. Rectifying features characterized by asymmetric I-V curves are observed. With decreasing temperature, the current decreases in the forward bias side and under the low voltages in the reverse bias side, while the current first increases down to ~100 K and then decreases under the high voltages in the reverse bias side. Similar notable phenomenon in the negative bias voltage side has also been observed in the $La_{0.9}Hf_{0.1}MnO_3$/Nb-doped $SrTiO_3$ heterojunction.[26] This unusual feature occurs at ~100 K, close to the metal-insulator transition temperature and the crossover temperature of the

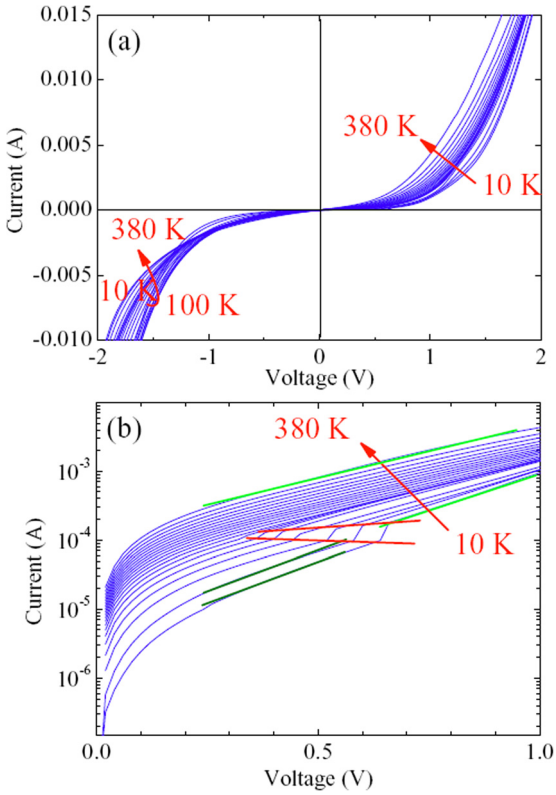

FIG. 5. (a) Current-voltage characteristics of CCO/SNTO heterojunction in a wide temperature range from 10 K to 380 K with a temperature step of 20 K. (b) Semilogarithmic plot of the forward bias region of the *I-V* characteristics. Green and olive lines are linear fits. Red line marks the boundary between two electrical processes. Arrows are the guides for the eyes.

unusual measured temperature dependence of the Hall coefficient of the CCO film. Therefore, we believe that this unusual *I-V* feature is related to the change the concentration of the hole carriers of the CCO side at around 100 K, from the fact that the concentration of the hole carriers smoothly increases with decreasing temperature and then decreases across 100 K. On the other hand, in the conventional *p-n* junctions, electrons in the valence band on the *p* side can directly tunnel to the empty states in the *n* side under an applied reverse bias voltage, which process is called the interband Zener tunneling.[27] While in the transition-metal oxide *p-n* junctions, the trap assisted tunneling process assisted by the oxygen-vacancy-induced states was proposed to be the dominant transport mechanism.[28]

To gain the information on the transport mechanism of the junction, the *I-V* curves were further analyzed. The semilogarithmic plot of the *I-V* characteristics under forward bias was shown in Fig. 5(b). From Fig. 5(b), one can see that the characteristics of the *I-V* curves can be classified into two regimes according to a single electrical process or duplicate processes between different temperature ranges. Between 380-100 K, a simple linearity of the Log*I-V* relation is observed, indicating a single electrical process. While below 100 K, a second electrical process occurs. This critical temperature ~100 K is also close to the metal-insulator transition temperature and the crossover temperature of the measured unusual temperature dependence of the Hall coefficient of the CCO film. Between 380 to 100 K, a single linear relation between *LogI* and *V* is observed. The slope of the *LogI* versus *V* is almost temperature independent and the Log*I* increases linearly with temperature when the electric bias is fixed, indicating that the charge carrier tunneling occurs predominantly through a potential barrier. In fact, in the temperature range from 380 to 100 K, the CCO shows the metallic-like behavior, and Nb-doped $SrTiO_3$ (0.7 wt. % doped) is an *n*-type degenerate semiconductor, therefore, a Schottkey barrier could be formed. Because the carrier concentrations of the CCO films ($\sim 4.3 \times 10^{20}\,cm^{-3}$) and of the SNTO ($\sim 10^{19} \sim 10^{20}\,cm^{-3}$) are generally large and the barrier width is correspondingly thin in transition-metal oxide heterojunctions comparing the conventional semiconductor heterojunctions, charge carriers can easily tunnel through the potential barrier to cross the junction instead of surmounting

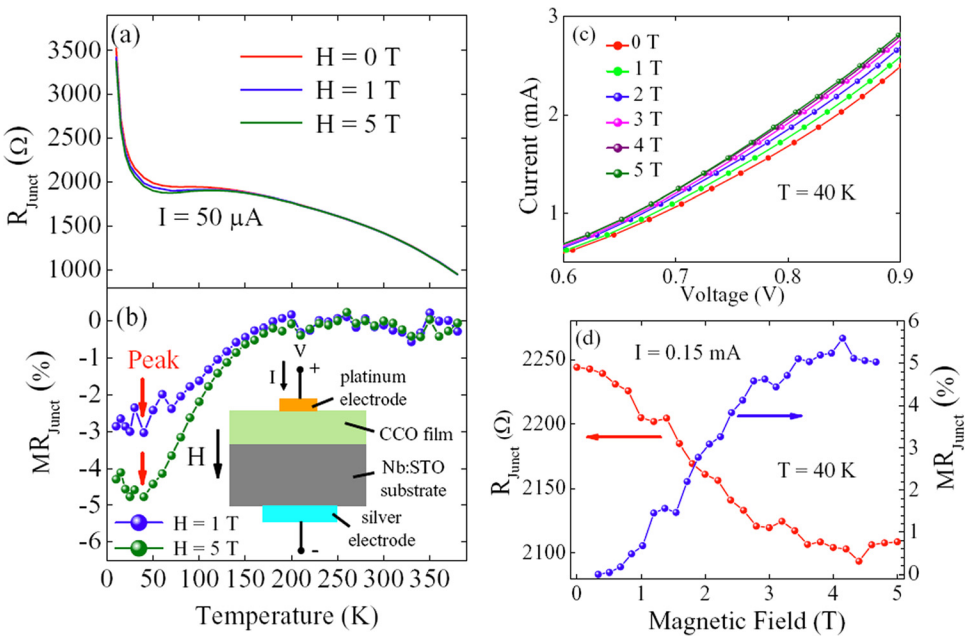

FIG. 6. (a) Temperature dependence of the junction conductive resistance (R_{Junct}) of the CCO/SNTO *p-n* junction, measured with a current of 50 μA and in the different magnetic fields ($H = 0$, 1, and 5 T). (b) Magnetoresistance (MR_{Junct}) for the CCO/SNTO *p-n* junction. (c) CCO/SNTO *p-n* junction current as a function of positive bias at 40 K in varying magnetic field. (d) Dependence of the MR_{Junct} ratio and junction resistance R_{Junct} of the CCO/SNTO *p-n* junction on magnetic field at 40 K, measured with a current of 0.15 mA. Inset in Fig. 6(b) shows the schematic illustrations of the CCO/SNTO junction.

the potential barrier by thermal activating charge carriers. In the latter case, the *LogI-V* slope is expected to vary with $1/T$, the temperature plays an important role in activating charge carriers. If the tunneling occurs predominantly, the forward current can be described by Newman equation: $I = I_s\exp(\alpha T)\exp(\beta V)$, where I_s, α, and β are parameters weakly depending on V.[29] From the Newman equation, temperature-independent slope in the *LogI-V* characteristics can be predicted and *LogI* linearly increases with temperature if the applying electric bias is fixed. The results show that the slope of the *LogI* versus V is almost temperature independent under forward bias in the high temperature range, strongly deviating from the thermionic emission mechanism and qualitatively consistent with tunneling process.

In the temperature range below 100 K, two-process phenomena in the CCO/STO heterojunction are observed. There is a critical voltage (V_c) that divides the *LogI-V* curves into two linear segments with slight different slope, and this slight difference between two slope decreases with increasing temperature from 10 K and disappears at around 100 K. At low bias regime, the linear relation between *LogI* and V is also observed, and the slope of the *LogI* versus V is almost temperature independent, indicating that the low-bias process also follows the tunneling mechanism. At high bias range, the excellent linear relation between *LogI* and V could be obtained while the slope of *LogI-V* characteristics decreases as temperature increases from 10 K to 100 K, indicating the combined thermionic emission-diffusion process.[30,31] High-resolution photoemission spectroscopy demonstrated that the density of states in the CCO at E_F gradually decreases with decreasing temperature below 100 K, and that an energy gap eventually opens across E_F at a temperature below 50 K.[32] At the temperature range 10-100 K, CCO shows semiconducting behavior, and a (*p*-type)- CCO-(*n*-type)SNTO heterojunction should be constructed. For simplicity of analysis and drawing schematic potential profile of the CCO/SNTO junctions, we assume hereafter that most of the depletion layer developed in the *n*-type Nb:STO layer. This assumption is reasonable because we can take into account the fact that the carrier concentration is generally large and the barrier width is correspondingly thin in the CCO side.

The transport behavior of the CCO/SNTO *p-n* junction was measured under applied magnetic fields varying between 0 and 5 T and a temperature range of 10-380 K by PPMS. Figure 6(a) shows the temperature dependence of the junction conductive resistance (R_{Junct}) measured in the different magnetic fields ($H = 0$, 1, and 5 T). Notice that the junction conductive resistance almost shows a semiconducting-like behavior in the measuring temperature range, except it shows a small reentrant behavior below 100 K. Similar temperature dependence of semiconducting-like conductive behavior also has been observed in the transverse transport (ρ_c) measurements of CCO single crystal.[15] The difference of the in-plane transport property of the CCO film and the junction transport property of the CCO junction maybe comes from the anisotropic nature of transport properties in CCO single crystal with layered structure.[9] Magnetoresistances (*MR*) of the CCO/SNTO junction at different temperature are shown in Fig. 6(b). The MR is defined as $MR_{Junct} = [R_{(H)}\text{-}R_{(0)}]/R_{(0)}$. The magnetic field H was applied perpendicular to the interfaces of the heterojunction and parallel to the current. Negative MR_{Junct} is observed below ~200 K in the CCO/SNTO heterojunction. Its magnitude increases as temperature decreases, and exhibits a peak at 40 K, as shown in Fig. 6(b), close to the short-range to long-range IC-SDW transition temperature (~30 K) in bulk. Therefore, we have reason to believe that this temperature of the minimum MR value is associated with the temperature of the short-range to long-range IC-SDW transition in CCO. The temperature dependences of MR_{Junct} in the field of 1 and 5 T both exhibit a peak at 40 K. At 40 K, the dependence of the junction current on the applied magnetic field varying from 0 to 5 T were measured, as shown in Figure 6(c). Figure 6(d) shows very clearly that the junction resistance R_{Junct} decreases and the MR_{Junct} ratio increases with increasing magnetic field at this temperature. The negative MR in CCO/SNTO heterojunction is considered to be related to the CCO layer. Considering the alternating stacking structure of $Ca_3Co_4O_9$ along the *c* axis and interlayer magnetic coupling between the $[Ca_2CoO_3]$ and $[CoO_2]$ subsystems, the negative MR maybe originates from the decreases of spin scattering as a consequence of applied magnetic field. The negative MR maybe also comes from the suppression of SDW by magnetic field, since the larger negative MR was observed below 100 K, where the existence of an incommensurate spin-density-wave state with wide transition width (about $\Delta T = 70$ K).[9,17] On the other hand, X-ray absorption and photoemission investigations of the $Ca_3Co_4O_9$ showed that the hole-doped Co-O triangular lattice has Co^{4+} (low spin, $S = 1/2$) species in the nonmagnetic Co^{3+} (low-spin, $S = 0$) background, and the layered cobaltite system tends to be separated into hole-rich and hole-poor domains.[27] The hole-rich domain is a good metal, while the hole-poor domain is insulating probably due to carrier localization. The oxygen vacancies existing in the CCO layer grown by PLD induce a partial disproportionation of Co ions. Phase-separation scenario of the inhomogeneous distribution of the mixed-valence Co ion and oxygen vacancies in the CCO layer maybe affects magnetic-field dependent transport properties of the CCO/SNTO junction, inducing negative MR effect at low temperature. Similar phenomena of the phase-separation scenario inducing negative MR effects have been observed in the perovskite manganites, and the largest negative MR is observed in the vicinity of phase transition temperature.

IV. SUMMARY

In summary, thermoelectric cobalt $Ca_3Co_4O_9$ epitaxial heterostructures were fabricated by PLD. The measurements of in-plane resistivity, thermopower, and magnetic properties performed on the CCO thin films were found to be comparable to *ab*-plane those of the single crystals due to good orientation of the films. The temperature dependence of the resistance of the CCO film exhibits a transport crossover from the high-temperature metallic-like regime to the low-temperature insulating-like behavior below 100 K. The broad crossover of the temperature dependence of the Hall coefficient also occurs at around 100 K. Correspondingly, the

temperature dependent I-V characteristics of the CCO/SNTO heterojunctions show two distinctive transport mechanisms above and below 100 K. The junction exhibits negative magnetoresistance at low temperatures, and the mechanism is discussed.

ACKNOWLEDGMENTS

This work was supported by the National Basic Research Program of China (Grant No. 2012CB921403), the National Natural Science Foundation of China (Grant No 10904030, 11004238, and 11134012), and Direction Program of Knowledge Innovation of Chinese Academy of Sciences (Grant No. YOV2021L31).

[1]S. Jin, T. H. Tiefel, M. McCormack, R. A. Fastnacht, R. Ramesh, and L. H. Chen, Science **264**, 413 (1994).
[2]S. D. Bader, Rev. Mod. Phys. **78**, 1 (2006).
[3]K. J. Jin, H. B. Lu, Q. L. Zhou, K. Zhao, B. L. Cheng, Z. H. Chen, Y. L. Zhou, and G. Z. Yang, Phys. Rev. B **71**, 184428 (2005).
[4]K. J. Jin, H. B. Lu, K. Zhao, C. Ge, M. He, and G. Z. Yang, Adv. Mater. **21**, 4636 (2009).
[5]P. Kumar, Nanosci. Res. Lett. **5**, 1596 (2010).
[6]P. Kumar, M. G. Krishna, and A. K. Bhattacharya, Bull. Mater. Sci. **32**, 263 (2009).
[7]M. N. Baibich, J. M. Broto, A. Fert, F. Nguyen Van Dan, and F. Petroff, Phys. Rev. Lett. **61**, 2472 (1988).
[8]Y. Tomioka, A. Asamitsu, Y. Moritomo, H. Kuwahara, and Y. Tokura, Phys. Rev. Lett. **74**, 5108 (1995).
[9]H. Habermeier, Mater. Today **10**, 34 (2007).
[10]S. J. May, P. J. Ryan, J. L. Robertson, J.-W. Kim, T. S. Santos, E. Karapetrova, J. L. Zarestky, X. Zhai, S. G. E. te Velthuis, J. N. Eckstein, S. D. Bader, and A. Bhattacharya, Nature Mater. **8**, 892 (2009).
[11]M. G. Krishna and P. Kumar, *Emerging Nanotechnologies for Manufacturing* (William Andrews Inc, New York, 2009).
[12]P. Kumar, M. G. Krishna, A. K. Bhatnagar, and A. K. Bhattacharya, J. Mater. Res. **23**, 1826 (2008).
[13]G. Logvenov, A. Gozar, and I. Bozovic, Science **326**, 699 (2009).
[14]O. Ohtom and H. Huang, Nature **427**, 423 (2004).
[15]A. C. Masset, C. Michel, A. Maignan, M. Hervieu, O. Toulemonde, F. Studer, B. Raveau, and J. Hejtmanek, Phys. Rev. B **62**, 166 (2000).
[16]R. Venkatasubramanian, E. Siivola, T. Colpitts, and B. O'Quinn, Nature **413**, 597 (2001).
[17]S. F. Wang, A. Venimadhav, S. M. Guo, K. Chen, Q. Li, M. D. Vaudin, and X. X. Xi, Appl. Phys. Lett. **94**, 022110 (2009).
[18]X. Zhu, D. Shi, S. Dou, Y. Sun, Q. Li, L. Wang, W. Li, W. Yeoh, R. Zheng, Z. Chen, and C. Kong, Acta Mater. **58**, 4281 (2010).
[19]Q. Qiao, A. Gulee, T. Paulauskas, S. Kolesnik, B. Dabrowski, M. Ozdemir, C. Boyraz, D. Mazumdar, A. Gupta, and R. F. Klie, J. Phys.: Condens. Matter **23**, 305005 (2011).
[20]Takeuchi, T. Kondo, T. Takami, H. Takahashi, H. Ikuta, U. Mizutani, R. Funahashi, M. Shikano, M. Mikami, S. Tsuda, T. Yokoya, S. Shin, and T. Muro, Phys. Rev. B **69**, 125410 (2004).
[21]Y. Miyazaki, K. Kudo, M. Akoshima, Y. Ono, Y. Koike, and T. Kajitani, Jpn. J. Appl. Phys., Part 2 **39**, L531 (2000).
[22]H. W. Eng, P. Limelette, W. Prellier, Ch. Simon, and R. Frésard, Phys. Rev. B **73**, 033403 (2006).
[23]J. Sugiyama, H. Itahara, T. Tani, J. H. Brewer, and E. J. Ansaldo, Phys. Rev. B **66**, 134413 (2002).
[24]J. Sugiyama, J. H. Brewer, E. J. Ansaldo, H. Itahara, K. Dohmae, Y. Seno, C. Xia, and T. Tani, Phys. Rev. B **68**, 134423 (2003).
[25]J. Sugiyama, C. Xia, and T. Tani, Phys. Rev. B **67**, 104410 (2003).
[26]L. Wang and J. Gao, J. Appl. Phys. **105**, 07C904 (2009).
[27]C. Zener, Proc. R. Soc. Lond. A **145**, 523 (1934).
[28]P. Han, K. J. Jin, H. B. Lu, Y. L. Zhou, and G. Z. Yang, Appl. Phys. Lett. **91**, 182102 (2007).
[29]S. M. SZE, *Physics of Semiconductor Devices*, 2nd ed. (Wiley, New York, 1981).
[30]W. M. Lü, J. R. Sun, Y. Z. Chen, and B. G. Shen, Appl. Phys. Lett. **94**, 152514 (2009).
[31]W. M. Lü, J. R. Sun, D. J. Wang, Y. W. Xie, S. Liang, Y. Z. Chen, and B. G. Shen, Appl. Phys. Lett. **93**, 212502 (2008).
[32]T. Takeuchi, T. Kondo, T. Takami, H. Takahashi, H. Ikuta, U. Mizutani, K. Soda, R. Funahashi, M. Shikano, M. Mikami, S. Tsuda, T. Yokoya, S. Shin, and T. Muro, Phys. Rev. B **69**, 125410 (2004).